

ARTICLE OPEN



Controlling crystal-electric field levels through symmetry-breaking uniaxial pressure in a cubic super heavy fermion

Elena Gati¹, Burkhard Schmidt¹, Sergey L. Bud'ko^{2,3}, Andrew P. Mackenzie^{1,4} and Paul C. Canfield^{2,3}

YbPtBi is one of the heavy-fermion systems with largest Sommerfeld coefficient γ and is thus classified as a ‘super’-heavy fermion material. In this work, we resolve the long-debated question about the hierarchy of relevant energy scales, such as crystal-electric field (CEF) levels, Kondo and magnetic ordering temperature, in YbPtBi. Through measurements of the a.c. elastocaloric effect and generic symmetry arguments, we identify an *elastic level splitting* that is unambiguously associated with the symmetry-allowed splitting of a quartet CEF level. This quartet, which we identify to be the first excited state at $\Delta/k_B \approx 1.6$ K above the doublet ground state at ambient pressure, is well below the proposed Kondo temperature $T_K \approx 10$ K. Consequently, this analysis of the energy scheme can provide support models that predict that the heavy electron mass is a result of an enhanced degeneracy of the CEF ground state, i.e., a quasi-sextet in YbPtBi. At the same time, our study shows the potential of the a.c. elastocaloric effect to control and quantify strain-induced changes of the CEF schemes, opening a different route to disentangle the CEF energy scales from other relevant energy scales in correlated quantum materials.

npj Quantum Materials (2023)8:69; <https://doi.org/10.1038/s41535-023-00596-1>

INTRODUCTION

An enhanced effective electron mass m^* is considered as a hallmark of a large class of strongly correlated metals. In such heavy-electron systems, many exotic quantum phenomena, including unconventional superconductivity, non-Fermi-liquid behavior, quantum criticality, and even topological semimetals^{1–7} occur. Among the materials with the largest Sommerfeld coefficients $\gamma \propto m^*$ are the rare-earth-based heavy fermion systems YbPtBi^{8,9}, YbT₂Zn₂₀ (T = Fe, Co)¹⁰ and PrAg₂In¹¹, also dubbed as ‘super’-heavy electron systems^{12,13}. In these cubic systems, γ reaches record values as high as $10 \text{ Jmol}^{-1} \text{ K}^{-2}$. The Yb-variants have in common that they are characterized by small characteristic energy scales^{10,14} of the order of $k_B \cdot 1 \dots 10$ K, including the Kondo scale $k_B T_K$ as well as excited crystal electric field (CEF) levels at $k_B T_{\text{CEF}}$. Correspondingly, it has been suggested that the hybridization of the conduction electrons¹ with a large number of degenerate CEF states is the source of the high electronic mass^{10,15,16}. However, given the multitude of small energy scales, a definite determination of the energy scales and thus a quantitative description of the unusually high γ has proven difficult^{14,17,18}.

For YbPtBi, specifically, the following characteristic temperature scales^{8,9,14,17,19,20} have been found so far (see Fig. 1a, c, d). Since the Yb³⁺ Kramers ion resides on a site with cubic symmetry, the CEF is expected to split the $J = 7/2$ multiplet into two doublets of type Γ_6 and Γ_7 and a Γ_8 quartet²¹. The analyses of several experiments consistently find that the highest CEF excited state is a doublet (likely Γ_6) with $T_{\text{CEF},2} \sim 60 \dots 100$ K. Even though various studies²⁰ favor Γ_7 to be the ground state and Γ_8 to be the first excited state with $T_{\text{CEF},1} \sim 1 \dots 10$ K, the reverse assignment with a Γ_8 ground state was also found to be compatible with a number of experimental results²⁰. In addition, symmetry-breaking distortions at low temperature, giving rise to additional level splittings, could not be conclusively ruled out so far^{17,20,22,23}. These uncertainties

have not only hampered estimates for the absolute value of $T_{\text{CEF},1}$, but also of the second important temperature scale T_K ¹⁴ which is believed to be in the same energy range. Finally, for very low temperatures below $T_N \approx 400$ mK, YbPtBi orders antiferromagnetically. This order is fragile^{12,24–26} as it can be suppressed towards a quantum critical point by a small external magnetic field, and non-Fermi-liquid behavior was discovered in the quantum critical region²⁴.

In this paper, we clarify the hierarchy of energy scales in YbPtBi, something only made possible through conducting thermodynamic measurements of the elastocaloric effect under well-controlled, symmetry-breaking, uniaxial pressure p . In contrast to magnetic field, which breaks time-reversal symmetry and thus affects all Kramers-degenerate states, the lattice strain ϵ associated with uniaxial pressure can only lift degeneracies stabilized by crystallographic symmetries. As we will show below, it is through this *elastic level splitting* that the application of uniaxial pressure can be used to sensitively probe the single-ion physics²⁷ associated with the Γ_8 state. As a result, we successfully disentangle the thermodynamic features resulting from CEF excitations and other energy scales which can be attributed to the Kondo scale in YbPtBi. Overall, this analysis, in line with literature results, places the ‘super’-heavy YbPtBi in the limit of $T_K > T_{\text{CEF},1}$ and provides support for the notion that the extremely high γ value results from the hybridization of conduction electrons with a quasi-sextet CEF ground state.

RESULTS

Experimental elastocaloric effect data

The elastocaloric effect $\Delta T/\Delta \epsilon$ describes a temperature change ΔT that is induced by varying the strain by $\Delta \epsilon$.

¹Max Planck Institute for Chemical Physics of Solids, 01187 Dresden, Germany. ²Ames National Laboratory, US Department of Energy, Iowa State University, Ames, IA 50011, USA.

³Department of Physics and Astronomy, Iowa State University, Ames, IA 50011, USA. ⁴Scottish Universities Physics Alliance, School of Physics and Astronomy, University of St Andrews, St Andrews, UK. ✉email: elena.gati@cpfs.mpg.de

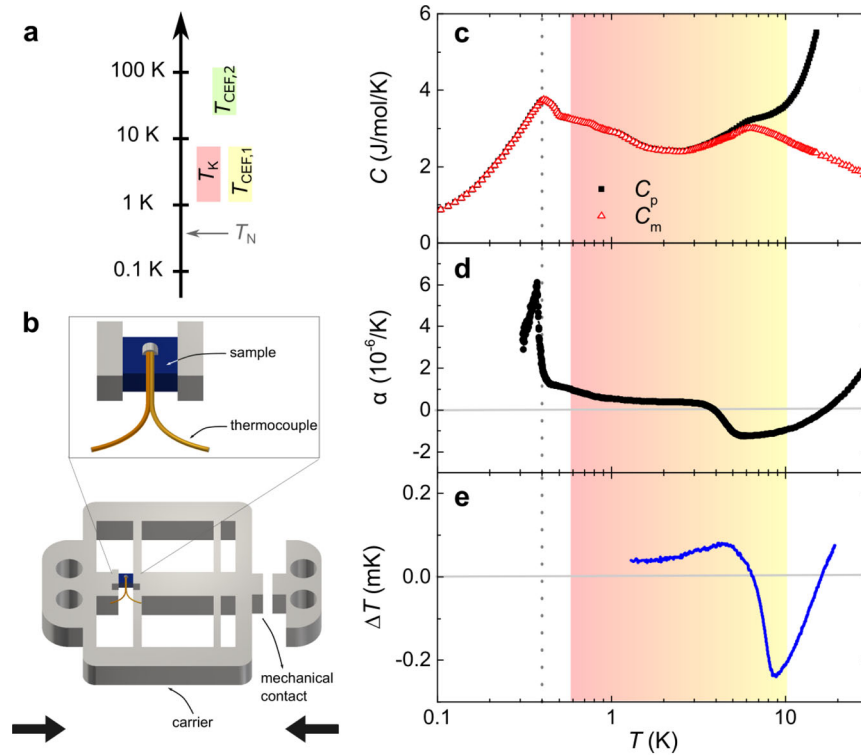


Fig. 1 Ambient-pressure thermodynamics of YbPtBi. **a** Schematic representation of proposed characteristic energy scales of YbPtBi. T_N indicates the temperature of magnetic ordering, T_K the possible temperature range of the Kondo crossover and $T_{\text{CEF},1}$ and $T_{\text{CEF},2}$ the possible temperature range of the first and second excited crystal-electric field levels. **b** Schematic of the setup to measure the elastocaloric effect²⁸. A sample with attached thermocouple is placed across a gap on the sample carrier, which is screwed into the pressure cell (not shown). Different compressive uniaxial pressures can be exerted when the mechanical contact is closed by a uniaxial pressure cell. The direction of applied force is indicated by the big black arrows. The strain-induced temperature changes, ΔT , are recorded with the thermocouple. **c–e** Ambient-pressure properties of YbPtBi: total specific heat, C_p , and magnetic specific heat, C_m ²⁴, (c) thermal expansion²⁴, α , (d) and elastocaloric temperature amplitude, ΔT (e), from this work. The highlighted temperature range indicates the temperature range of the Kondo/crystal-electric field scales, and the dotted line indicates T_N , as also shown in (a).

Thermodynamically it is given by

$$\left. \frac{\Delta T}{\Delta \epsilon} \right|_S = - \frac{\partial S / \partial \epsilon|_T}{\partial S / \partial T|_e} = - \frac{T}{C_V} \frac{\partial S}{\partial \epsilon} \Big|_T, \quad (1)$$

with S being the entropy and C_V the heat capacity at constant volume V .

As recently established in ref. ²⁸, $\Delta T / \Delta \epsilon$ can be determined with high precision in an a.c. version of the technique by applying an oscillation with amplitude $\Delta \epsilon$ in piezo-driven uniaxial pressure cells^{29,30} and measuring the resulting ΔT using a thermocouple (see Fig. 1b). $\Delta \epsilon$ is determined through a capacitive displacement sensor (not shown). A constant, finite strain ϵ can be superimposed, so that $\Delta T / \Delta \epsilon$ can be mapped out as a function of ϵ . In this work, we follow this experimental method to determine $\Delta T / \Delta \epsilon$ for YbPtBi with uniaxial pressure p applied along the crystallographic [1 0 0] direction, resulting in a finite ϵ . We implemented following important modifications to the technique: first, we use a uniaxial pressure cell that also incorporates a force sensor²⁹ since the applied force/pressure p is a better control parameter than the conjugated strain ϵ in these type of devices. Second, we mount the sample free-standing in a sample carrier which is designed in such a way that only compression (denoted by a negative sign of p) can be applied when the mechanical contact in the carrier is closed (see Fig. 1b, ref. ³¹). This allows us to determine precisely the neutral point $p = 0$ (and $\epsilon = 0$) at any given temperature which is important for the symmetry arguments presented below.

To illustrate the fingerprint of relevant energy scales in YbPtBi at ambient pressure in our data, we first compare on the right of

Fig. 1 the elastocaloric temperature amplitude $\Delta T(T)$ for $T \gtrsim 1.2$ K (panel (e)) at ambient pressure $p_a \approx 0$ and $\Delta \epsilon \approx \text{const.}$ with literature data²⁴ on the molar specific heat $C_p(T) \propto T \partial S / \partial T|_{p_a}$ (panel (c)) and the thermal expansion $\alpha(T) \propto \partial S / \partial p|_T \propto \partial S / \partial \epsilon|_T$ (panel (d)) (see Supplementary Note 2 for a discussion of the equivalence of different thermodynamic quantities at ambient pressure). Upon cooling, ΔT shows a clear feature around $T^* \approx 7.6$ K (see Supplementary Note 1 for criterion) with a concomitant sign change of ΔT . $\alpha(T)$ also exhibits a similar feature as $\Delta T(T)$, including a sign change, at a slightly lower temperature. Simultaneously, the magnetic contribution C_m to the specific heat C_p , obtained after subtracting the specific heat of the non-moment bearing Lu analogue²⁴, shows a clear peak at T^* . Previously, these prominent features in α and C_m were interpreted either to be solely due to CEF effects or to combined CEF/Kondo effects. Here, we will provide an alternative interpretation, and we will show that the first excited CEF level is in fact located much lower in energy. Upon further cooling down to ≈ 1.2 K, the lowest temperature of our experiment, $\Delta T(T)$ remains featureless and small, similar to $\alpha(T)$. At even lower temperatures $C_p(T)$ and $\alpha(T)$ show clear features associated with a magnetic phase transition at $T_N \approx 0.4$ K.

Now we turn to the behavior of ΔT under finite, symmetry-breaking uniaxial pressure p , shown in Fig. 2. In our experiments, we were able to apply compression as high as ≈ -1.8 GPa, which is a large value for uniaxial compression in these devices³¹. Clearly, the data sets as a function of T (Fig. 2a) and p (Fig. 2b) reveal significant changes of $|\Delta T|$. Key observations can be summarized as follows: first, as $|p|$ is increased, a low-temperature extremum emerges at $T_{\text{ext}} \approx 2.7$ K for $p \approx -0.3$ GPa, which is increased to 4.0 K

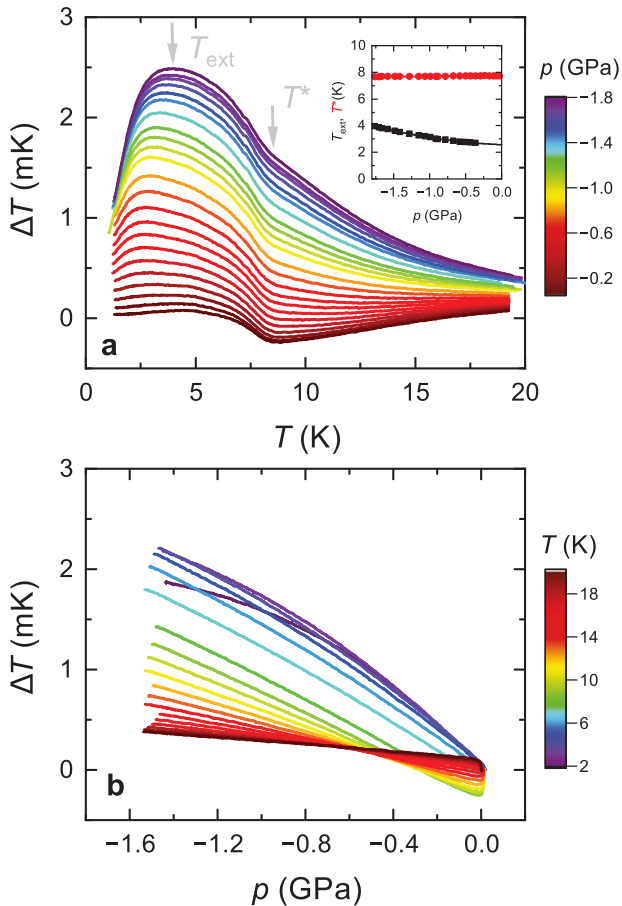


Fig. 2 Elastocaloric effect of YbPtBi under finite, symmetry-breaking uniaxial pressure. Elastocaloric temperature amplitude, ΔT , induced by a small oscillating uniaxial strain with amplitude $\Delta\epsilon \approx \text{const.} < 0$ at constant offset uniaxial pressures, p , as a function of temperature, T , **(a)** and as a function of p at constant T **(b)**. Note that the $p \approx 0$ data is also shown in Fig. 1 on a logarithmic T scale. The data spacing in **(a)** is ~ 0.1 GPa and in **(b)** 1 K (for $T < 10$ K) and 2 K (for $T > 10$ K). The arrows in panel **(a)** indicate the position of the characteristic temperatures T_{ext} and T^* . The inset to **(a)** shows the evolution of T_{ext} and T^* with p (for criteria, see Supplementary Note 1).

by $p \approx -1.8$ GPa. Second, the feature at $T^* \approx 7.6$ K remains visible for all pressures and its position is only barely affected by p (see inset of Fig. 2a). Third, ΔT increases strongly, from almost zero, in a monotonic and, to first approximation, in a near linear manner with $|p|$ for any given T . Only for larger $|p| \gtrsim 0.5$ GPa are some deviations from this p -linear behavior, in particular at lowest T , observed.

In general, this elastocaloric effect data contains contributions from all relevant energy scales, in particular the CEF and Kondo energy scales. In the following we will use generic qualitative arguments and explicit modeling of the elastocaloric effect of single-ion CEF states to disentangle these contributions. In particular, we will demonstrate that the strong change of temperature ΔT with uniaxial pressure p results from the response of the first excited quartet CEF level to symmetry breaking, whereas the behavior of ΔT at $p = 0$ (including the anomaly at T^*) most likely originates from the formation of the coherent Kondo state.

To facilitate the discussion of the elastocaloric effect of CEF levels, we will from now on focus on the notion of strain ϵ , since Young's modulus $Y_{100} := \partial p / \partial \epsilon|_T \approx \text{const.}$ (see Supplementary Note 5), and assume temperatures $T = \mathcal{O}(\Delta_{\text{CEF}}) / k_B$ where Δ_{CEF} is the

energy difference between ground state and first excited CEF energy level. The two dominant effects of finite ϵ are expected to be (i) shifting the CEF levels and (ii) a possible lifting of degenerate CEF levels due to lowering the crystal symmetry. The latter scenario will most likely only be relevant when the degenerate state is not the ground state, since the degeneracy is otherwise prone to be lifted already at zero strain through a spontaneous Jahn-Teller distortion or multipolar order^{32,33}. The elastocaloric effect $\Delta T / \Delta \epsilon$ is expected to be significantly distinct in these two cases.

The two scenarios are visualized separately in Fig. 3a: In case (i), left sketch of the figure, the CEF energy level is unambiguously associated with ϵ , necessary for the applicability of Grüneisen scaling $\partial p / \partial T|_V \propto C_V / V$ (see Supplementary Note 6). We obtain $\partial S / \partial \epsilon|_T \propto T \partial S / \partial T|_T$, therefore $\Delta T / \Delta \epsilon \approx \text{const.}$ as a function of strain, see Eq. (1). Thus, in this case, we expect a large intercept of $\Delta T / \Delta \epsilon$ at $\epsilon = 0$ and no significant change with ϵ .

In case (ii), the strain-induced symmetry lowering leads to a splitting of the first excited CEF energy level for both compressive and tensile strains. Hence, at $\epsilon = 0$ we must have $\partial S / \partial \epsilon|_T = 0$, correspondingly $\Delta T / \Delta \epsilon = 0$ and Grüneisen scaling is no longer applicable. We also must have $\partial S / \partial \epsilon|_T \propto \epsilon$. Therefore, in scenario (ii), we expect that the magnitude of $\Delta T / \Delta \epsilon$ is expected to increase rapidly from a small value at $\epsilon = 0$ with increasing tension or compression (see right sketch of Fig. 3a).

Our data (see Figs. 2 and 3c) is characterized by a large change of $\Delta T / \Delta \epsilon$ with ϵ and only a small finite intercept at $\epsilon = 0$. We can therefore conclude that the elastocaloric effect under finite strains is dominated by a strain-induced splitting of a first excited CEF level. This CEF level has to be the Γ_8 quartet, since the Yb^{3+} Kramers doublets are protected by time-reversal symmetry and cannot be split by the application of strain.

We note that these considerations also imply that measurements of the thermal expansion α at ambient pressure will only display anomalies of excited CEF levels when these levels are doublets that only shift with strain. In contrast, the excited CEF Γ_8 level will leave almost no fingerprint in $\alpha(p = 0) \propto \partial S / \partial \epsilon|_T (\epsilon = 0) \approx 0$ when the level splitting is the dominant effect. Therefore, a finite α seems unlikely to be related to the physics of the Γ_8 level, contrary to what has been discussed in previous studies on YbPtBi ¹⁷ under the assumption of validity of Grüneisen scaling (see Supplementary Note 6).

Modeling of the elastocaloric effect

To extract quantitative information on the CEF states from the elastocaloric data, in particular on the estimate of energy of the Γ_8 level in YbPtBi , we performed model calculations of $\Delta T / \Delta \epsilon$ using a simplified model with a minimal number of free parameters. Our model is based on a Schottky-type specific heat C_p of a two-level system with four-fold degenerate first excited state at energy Δ_{CEF} . We do not include a possible hybridization-induced broadening of the CEF levels, because (i) Kondo hybridization does not significantly change the energy levels of the f electrons and (ii) the applied stress yields an approximately volume conserving strain which only has a minor effect on the Kondo hybridization with the CEF levels as such. We note that only the occupation of the f electron energy levels, which is by definition only weakly affected by the Kondo coupling, is measured in our elastocaloric experiments. This is in contrast to spectroscopic experiments, where the single-particle spectral function is measured and thus the quasielastic linewidth is strongly broadened, which renders effects from the CEF level splitting unobservable. In addition, since our measured signal is $\Delta T \propto 1 / C_p$, we added an electronic contribution of the form γT to the total model specific heat C_p . To reduce the number of parameters, we omitted phononic contributions because they are small below ~ 10 K (see Fig. 1c). The full model specific heat at $\epsilon = 0$ is shown in the left panel of

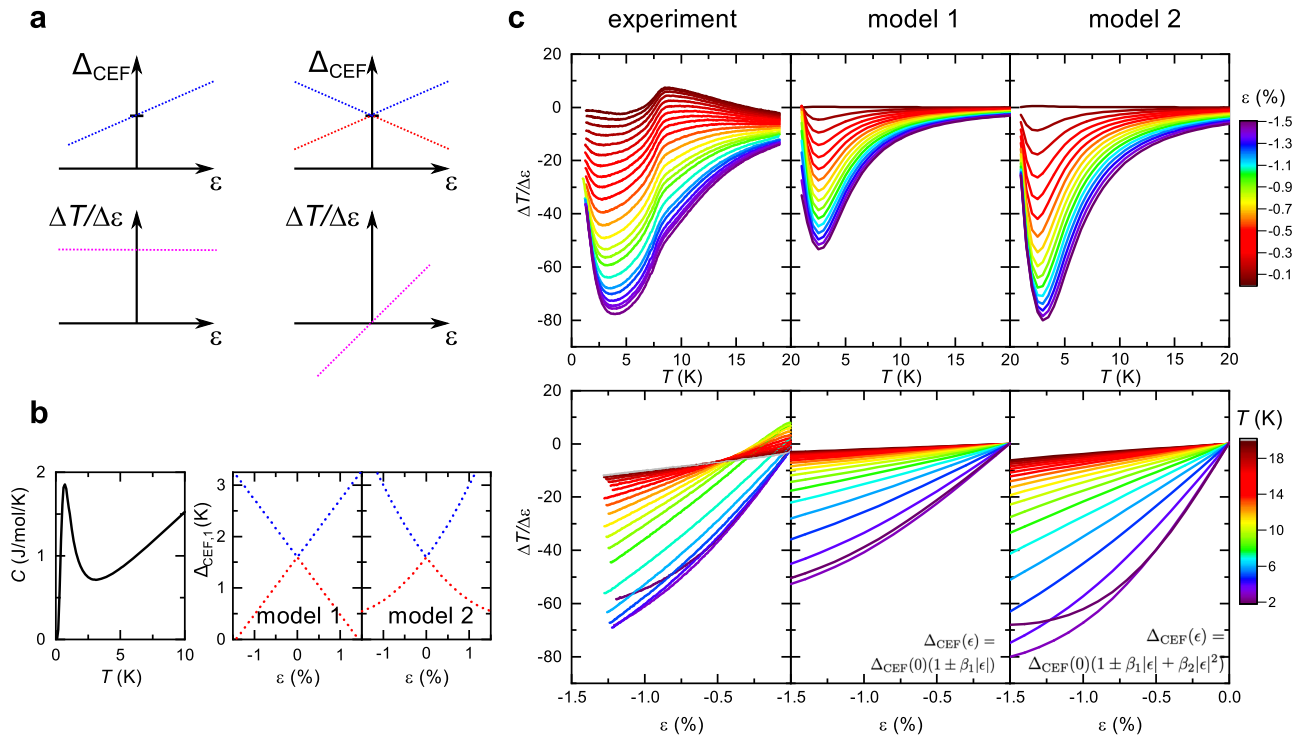


Fig. 3 Modeling of the elastocaloric effect of YbPtBi. **a** Generic considerations of the impact of a strain ϵ on the CEF energy level difference Δ_{CEF} and the resulting behavior of $\Delta T/\Delta\epsilon$ at constant temperature $T = \mathcal{O}(\Delta_{\text{CEF}})/k_{\text{B}}$. Left: scenario (i), induced shift of the first excited level. Right: scenario (ii), strain-induced splitting of the first excited level. **b** Left: model specific heat $C_p(T)$ at $\epsilon = 0$. Right: strain-induced splitting of Δ_{CEF} as a function of ϵ used in model 1 and model 2, both within scenario (ii) (see text for details). **c** Comparison of experimental data of the elastocaloric effect and the results of the two model calculations. For the experimental data, $Y_{100} \approx 120$ GPa was used⁴⁷ to express p in terms of ϵ (see text and SI). The data spacing for both experimental data and model calculations in the top panel is $\sim 0.08\%$ and in the bottom panel 1 K.

Fig. 3b. Using a value of $\Delta_{\text{CEF}}/k_{\text{B}} = 1.6$ K, this model reproduces the broad hump in the literature $C_p(T)$ data^{8,24} around $T \approx 800$ mK.

To parameterize the response to strain, we use two approximations, which we call model 1 and model 2. Model 1 comprises a linear splitting by strain via $\Delta_{\text{CEF}}(\epsilon) = \Delta_{\text{CEF}}(0)(1 \pm \beta_1|\epsilon|)$. The choice for this model is motivated by considering the effect of a tetragonal distortion on the CEF-Hamiltonian²¹ $\mathcal{H}_{\text{CEF}}^{\text{cubic}} \rightarrow \mathcal{H}_{\text{CEF}}^{\text{cubic}} + g_{\text{zz}}\epsilon O_2^0$ perturbatively with an elastic constant g_{zz} that characterizes the distortion and O_2^0 the Stevens operator that emerges in tetragonal symmetry (see Supplementary Note 8). The energy of the Γ_8 state then changes as $E_{\Gamma_8} \rightarrow E_{\Gamma_8} \pm 6g_{\text{zz}}\epsilon$ for small ϵ .

Naturally deviations from the ϵ -linear behavior of the CEF excitation energy will arise for larger $|\epsilon|$. In an attempt to better describe the magnitude of our experimental data, we include a second-order term of the expansion in ϵ in model 2. The corresponding energy splitting we use then reads $\Delta_{\text{CEF}}(\epsilon) = \Delta_{\text{CEF}}(0)(1 \pm \beta_1|\epsilon| + \beta_2|\epsilon|^2)$.

Figure 3c shows a comparison of the experimental data for $\Delta T/\Delta\epsilon$ (left column) to the calculations for model 1 (middle column) and model 2 (right column). For both models we use $\Delta_{\text{CEF}}(0)/k_{\text{B}} = 1.6$ K and $\beta_1 = 70$. Since the lowest temperature of our experiments is $T_{\text{min}} \approx 1.2$ K, we restrict the calculations to this temperature range. Therefore, the model results reflect the effects associated with the higher-energy branch (blue dotted lines in the right panel of Fig. 3b).

Clearly, the results for model 1 already capture many of the essential observations of the experiment on a qualitative level. It reproduces the low-temperature minimum of $\Delta T/\Delta\epsilon$ as a function of T around $T \approx 3$ K under finite ϵ , as well as the approximately linear change of $\Delta T/\Delta\epsilon$ with ϵ .

However, model 1 is not sufficient to account for the data also on a quantitative level. Repeating our calculations within model 2

and setting $\beta_2 = 1750$, we obtain the results shown in the right column of Fig. 3c). Now much of the experimental data can be very well reproduced over the full strain range.

Importantly, the good agreement between experiment and model calculations is only achieved when Γ_8 is the first excited state (scenario (ii)). In the Supplementary Note 7, we also show model calculations for the reverse scenario (we call it scenario (iii)) assuming Γ_8 is the ground state and the first excited state is a doublet, even if this scenario is unlikely due to the inherent instability of a symmetry-protected degeneracy of the ground state towards Jahn-Teller distortions. We find that scenario (ii) and (iii) can be clearly distinguished based on our experimental data by considering the value of T_{ext} for $\epsilon \rightarrow 0$. Specifically, we find that the finite value of T_{ext} for $\epsilon \rightarrow 0$ (see inset of Fig. 2a) is only compatible with scenario (ii). In fact, the value of T_{ext} for $\epsilon \rightarrow 0$ restricts the possible values of $\Delta_{\text{CEF}}(0)$, for which a reasonably good description of the experimental data within model 2 can be achieved. This leads us to estimate that $\Delta_{\text{CEF}}(0)/k_{\text{B}} = (1.6 \pm 0.3)$ K in YbPtBi.

DISCUSSION

Overall, our analysis establishes the Γ_8 quartet to be the first excited state with an energy difference to the doublet ground state of $\Delta_{\text{CEF}} \approx k_{\text{B}} \cdot 1.6$ K. However, the physics of single-ion CEF levels does not capture the feature at $T^* \sim 7.5$ K in $\Delta T/\Delta\epsilon$ which persists for all uniaxial pressures (see Fig. 2a and Fig. 3c). The model would also predict that $\Delta T/\Delta\epsilon \rightarrow 0$ for $\epsilon \rightarrow 0$, required by restoring the cubic crystal symmetry. Instead we observe a small but finite $\Delta T/\Delta\epsilon$, which we attribute to contributions from other energy scales than the Γ_8 one.

Since the remaining doublet CEF level excitation is located at much higher temperatures around 60...100 K, it can most likely be

excluded as the source for the anomaly at T^* . The remaining temperature scale which is known to be relevant in YbPtBi is set by the Kondo temperature T_K . Remarkably, the thermal expansion data²⁴ shown in Fig. 1d reveals the onset of negative α below $T \approx 20$ K that persists down to $T \approx T^*$. In general, a negative thermal expansion in cubic systems is exceptional³⁴. To rationalize this, we note that the volume of Yb^{3+} is smaller than the one of Yb^{2+} . Therefore, even tiny hybridization-induced changes^{35,36} of the strictly trivalent state of Yb can be the origin of a negative α . Thus, all experimental data are consistent with the expectations for the formation of the Kondo system with $T_K \approx T^* \approx 10$ K. However, solely based on the present elastocaloric data, we cannot entirely rule out the presence of yet another, so far undiscovered, characteristic energy scale in YbPtBi around $k_B T^*$.

From the analysis above, the hierarchy of temperature scales in YbPtBi can now be assigned to $T_{\text{CEF},2} > T^* > T_{\text{CEF},1}$. Therefore, this opens the possibility that the conduction electrons do not only hybridize with the Yb^{3+} CEF Γ_7 doublet ground state, but also with the first excited Γ_8 quartet state. Effectively, hybridization then takes place with an Yb quasi-sextet ($N=6$). This approximately matches the analysis¹⁵ of the generalized Kadowaki-Woods ratio A/γ^2 , with A being the Fermi-liquid coefficient of the resistivity, shows that $\rho(T)$ for YbPtBi^{8,10} falls between the values of A expected for $N=6$ and $N=8$. This is nonetheless remarkable for two reasons. First, for $T \ll T_{\text{CEF},1}$ the assumption of a quasi-sextet might be no longer valid. Second, the hybridization strength can also depend on the symmetry of the underlying CEF level^{37–40}, an aspect which has so far been rarely considered. Our study shows that YbPtBi with two low-lying CEF levels of different symmetry below $T^* \approx T_K$ might be an interesting reference system to quantify the relevance of symmetry-dependent hybridization strength. Based on the present results, an explicit modeling of the elastocaloric effect including all relevant degrees of freedom might be a promising pathway towards an improved quantitative description of the many-body physics in heavy fermions.

In summary, through measurements and analyses of the elastocaloric effect, we have firmly established the crystal-electric field levels and therefore the hierarchy of energy scales in the ‘super’-heavy fermion material YbPtBi. We find that the energy difference Δ_{CEF} between the ground state and the first excited quartet CEF level with $\Delta_{\text{CEF}} \approx k_B \cdot 1.6$ K is significantly smaller than the proposed Kondo scale $k_B T_K \approx k_B \cdot 10$ K, putting both the Γ_7 ground state doublet and the Γ_8 quartet below $k_B T_K$. This allows for the possibility that conduction electrons hybridize with a quasi-sextet ($N=6$) Yb^{3+} ground state, providing support for theoretical models that assign the anomalously large electron mass to an enhanced degeneracy of the CEF levels.

At a more general level, our work demonstrates that measurements of the elastocaloric effect under finite pressures^{41–44} enable us to control and quantify strain-induced changes of the crystal-electric field schemes and disentangle relevant low-energy scales in correlated electron systems. This approach will also be particularly relevant for the field of quantum magnets, in which the unambiguous determination of single-ion CEF states is essential for a microscopic description of their unusual magnetic properties.

METHODS

Crystal growth

Single crystals of YbPtBi were grown from ternary melts rich in Bi⁴⁵. High purity, elemental Yb, Pt, and Bi were combined in an alumina crucible in a 10(Yb):10(Pt):80(Bi) atomic ratio, sealed in an amorphous silica tube under 1/6 atmosphere of Ar and heated to 1100 °C over 4 h. After dwelling at 1100 °C for 3 h, the ampule was cooled to 900 °C over 2 h and then slowly cooled to 600 °C over 231 h. After dwelling at 600 °C for a few hours the ampule was taken out of the furnace, inverted into a metal centrifuge cup and rotated

a several thousand rpm for times less than 15 s⁴⁵ so as to separate the remaining, very Bi rich, remaining liquid from the grown YbPtBi crystals. The resultant crystals were well faceted and could be as large as 5–10 mm on a side. Given that YbPtBi is air sensitive, crystals were sealed in evacuated silica tubes for long-term storage.

Elastocaloric effect measurements

The samples were polished for measurements under finite uniaxial pressures²⁹ into a bar with dimensions of $100 \mu\text{m} \times 140 \mu\text{m} \times 1000 \mu\text{m}$, with the long axis being the strain axis. For measurements of the a.c. elastocaloric measurements, the d.c. voltages on the piezoelectric actuators were modulated by a small a.c. voltage with frequency $f = 56.13$ Hz (see Supplementary Note 4) on the tension stack. For the measurements of the induced temperature change ΔT , a chromel-AuFe_{0.07%} thermocouple⁴⁶ was fixed to the sample with a tiny amount of Stycast 1266 (see Supplementary Note 3). The thermocouple was anchored on the cell body. The voltage on the thermocouple was amplified by a low-temperature transformer mounted on the low-temperature stage and subsequently read out by a Lock-In amplifier. Further description on the uniaxial pressure cell and modeling of the elastocaloric effect are included in the main text (see Fig. 1).

DATA AVAILABILITY

The data that support the findings of this study are openly available in the Max Planck Digital Library under <https://doi.org/10.17617/3.KWANVF>.

CODE AVAILABILITY

The code used for our analyses are openly available in the Max Planck Digital Library under <https://doi.org/10.17617/3.KWANVF> together with the data.

Received: 8 May 2023; Accepted: 13 October 2023;

Published online: 20 November 2023

REFERENCES

- Stewart, G. R. Heavy-fermion systems. *Rev. Mod. Phys.* **56**, 755–787 (1984).
- Fulde, P., Keller, J. & Zwicknagl, G. in *Solid State Physics* Vol. 41, 1–150 (Elsevier, 1988).
- Zwicknagl, G. Quasi-particles in heavy fermion systems. *Adv. Phys.* **41**, 203–302 (1992).
- Thalmeier, P. & Zwicknagl, G. in *Handbook on the Physics and Chemistry of Rare Earths* Vol. 34, 135–287 (Elsevier, 2004).
- Gegenwart, P., Si, Q. & Steglich, F. Quantum criticality in heavy-fermion metals. *Nat. Phys.* **4**, 186–197 (2008).
- Paschen, S. & Si, Q. Quantum phases driven by strong correlations. *Nat. Rev. Phys.* **3**, 9–26 (2021).
- Mun, E. & Bud'ko, S. L. RPtBi: magnetism and topology. *MRS Bull.* **47**, 609–617 (2022).
- Fisk, Z. et al. Massive electron state in YbBiPt. *Phys. Rev. Lett.* **67**, 3310–3313 (1991).
- Canfield, P. C. et al. Magnetism and heavy fermion-like behavior in the RBiPt series. *J. Appl. Phys.* **70**, 5800–5802 (1991).
- Torikachvili, M. S. et al. Six closely related YbT₂Zn₂₀ (T = Fe, Co, Ru, Rh, Os, Ir) heavy fermion compounds with large local moment degeneracy. *Proc. Natl Acad. Sci. USA* **104**, 9960–9963 (2007).
- Yatskar, A., Beyermann, W. P., Movshovich, R. & Canfield, P. C. Possible correlated-electron behavior from quadrupolar fluctuations in PrInAg₂. *Phys. Rev. Lett.* **77**, 3637–3640 (1996).
- Canfield, P. C. & Bud'ko, S. L. Preserved entropy and fragile magnetism. *Rep. Prog. Phys.* **79**, 084506 (2016).
- Tokita, Y. et al. Super-heavy electron material as metallic refrigerant for adiabatic demagnetization cooling. *Sci. Adv.* **2**, e1600835 (2016).
- Canfield, P. et al. Groundstate properties of YbBiPt. *Phys. B: Condens. Matter* **197**, 101–108 (1994).
- Tsujii, N., Kontani, H. & Yoshimura, K. Universality in heavy Fermion systems with general degeneracy. *Phys. Rev. Lett.* **94**, 057201 (2005).

16. Shimura, Y. et al. Fragile superheavy Fermi liquid in $\text{YbCo}_2\text{Zn}_{20}$. *Phys. Rev. B* **101**, 241102 (2020).
17. Ueland, B. G. et al. High-resolution x-ray diffraction study of the heavy-fermion compound YbBiPt . *Phys. Rev. B* **92**, 184111 (2015).
18. Ivanshin, V. et al. Electron spin resonance of dense Yb-based heavy-fermion compounds: new experimental data. *J. Alloy. Compd.* **480**, 126–127 (2009).
19. Robinson, R. et al. Crystal field levels in YbBiPt . *Phys. B: Condens. Matter* **186–188**, 550–552 (1993).
20. Robinson, R. A. et al. Low-energy excitations and the electronic specific heat of YbBiPt . *Phys. Rev. Lett.* **75**, 1194–197 (1995).
21. Lea, K., Leask, M. & Wolf, W. The raising of angular momentum degeneracy of f-Electron terms by cubic crystal fields. *J. Phys. Chem. Solids* **23**, 1381–1405 (1962).
22. Robinson, R., Christianson, A., Nakotte, H., Beyermann, W. & Canfield, P. Low-energy excitations, symmetry breaking and specific heat in YbBiPt . *Phys. B: Condens. Matter* **259–261**, 138–139 (1999).
23. Martins, G. B. et al. Electron spin resonance of Er^{3+} in YBiPt . *Phys. Rev. B* **52**, 15062–15065 (1995).
24. Mun, E. D. et al. Magnetic-field-tuned quantum criticality of the heavy-fermion system YbPtBi . *Phys. Rev. B* **87**, 075120 (2013).
25. Ueland, B. G. et al. Fragile antiferromagnetism in the heavy-fermion compound YbBiPt . *Phys. Rev. B* **89**, 180403 (2014).
26. Movshovich, R., Lacerda, A., Canfield, P. C., Thompson, J. D. & Fisk, Z. Low-temperature phase diagram of YbBiPt . *J. Appl. Phys.* **76**, 6121–6123 (1994).
27. Lüthi, B. *Physical Acoustics in the Solid State*, Vol. 148, 1st edn (Springer, 2005).
28. Ikeda, M. S. et al. AC elastocaloric effect as a probe for thermodynamic signatures of continuous phase transitions. *Rev. Sci. Instrum.* **90**, 083902 (2019).
29. Barber, M. E., Steppke, A., Mackenzie, A. P. & Hicks, C. W. Piezoelectric-based uniaxial pressure cell with integrated force and displacement sensors. *Rev. Sci. Instrum.* **90**, 023904 (2019).
30. Hicks, C. W., Barber, M. E., Edkins, S. D., Brodsky, D. O. & Mackenzie, A. P. Piezoelectric-based apparatus for strain tuning. *Rev. Sci. Instrum.* **85**, 065003 (2014).
31. Jerzembeck, F. et al. The superconductivity of Sr_2RuO_4 under c-axis uniaxial stress. *Nat. Commun.* **13**, 4596 (2022).
32. Thalmeier, P., Akbari, A. & Shiina, R. in *Rare-Earth Borides* (ed. Inosov, D. S.) 603–677 (Jenny Stanford Publishing, 2021).
33. Vinograd, I. et al. Second order Zeeman interaction and ferroquadrupolar order in TmVO_4 . *npj Quantum Mater.* **7**, 68 (2022).
34. Mazzone, D. G. et al. Kondo-induced giant isotropic negative thermal expansion. *Phys. Rev. Lett.* **124**, 125701 (2020).
35. Brandt, N. & Moshchalkov, V. Concentrated Kondo systems. *Adv. Phys.* **33**, 373–467 (1984).
36. Kummer, K. et al. Similar temperature scale for valence changes in Kondo lattices with different Kondo temperatures. *Nat. Comm.* **9**, 2011 (2018).
37. Vyalikh, D. V. et al. k Dependence of the crystal-field splittings of 4f states in rare-earth systems. *Phys. Rev. Lett.* **105**, 237601 (2010).
38. Dong, R., Wan, X., Dai, X. & Savrasov, S. Y. Orbital-dependent electronic masses in Ce heavy-fermion materials studied via Gutzwiller density-functional theory. *Phys. Rev. B* **89**, 165122 (2014).
39. Rahn, M. C. et al. Kondo quasiparticle dynamics observed by resonant inelastic x-ray scattering. *Nat. Commun.* **13**, 6129 (2022).
40. Kang, B., Choi, S. & Kim, H. Orbital selective kondo effect in heavy fermion superconductor UTe_2 . *npj Quantum Mater.* **7**, 64 (2022).
41. Ikeda, M. S. et al. Elastocaloric signature of nematic fluctuations. *Proc. Natl Acad. Sci. USA* **118**, e2105911118 (2021).
42. Li, Y.-S. et al. Elastocaloric determination of the phase diagram of Sr_2RuO_4 . *Nature* **607**, 276–280 (2022).
43. Ye, L. et al. Elastocaloric signatures of symmetric and antisymmetric strain-tuning of quadrupolar and magnetic phases in DyB_2C_2 . *Proc. Natl Acad. Sci. USA* **120**, e2302800120 (2023).
44. Rosenberg, E. W., Chu, J.-H., Ruff, J. P. C., Hristov, A. T. & Fisher, I. R. Divergence of the quadrupole-strain susceptibility of the electronic nematic system YbRu_2Ge_2 . *Proc. Natl Acad. Sci. USA* **116**, 7232 (2019).
45. Canfield, P. C. New materials physics. *Rep. Prog. Phys.* **83**, 016501 (2019).
46. Stockert, U. & Oeschler, N. Thermopower of chromel-AuFe_{0.07%} thermocouples in magnetic fields. *Cryogenics* **51**, 154–155 (2011).
47. Oguchi, T. Electronic band structure and structural stability of LaBiPt . *Phys. Rev. B* **63**, 125115 (2001).

ACKNOWLEDGEMENTS

We acknowledge useful discussions with P. Thalmeier and thank E. Mun and B. Kuthanazhi for providing the ambient-pressure thermodynamic data. We also acknowledge the Gordon and Betty Moore Foundation for funding the International Workshop “Experimental Advances in the Use of Pressure and Strain to Probe and Control Quantum Matter”, which initiated the idea for this project. PCC acknowledges G. Wells for not letting YbPtBi be called a “morbidly obese Fermion”. Financial support by the Max Planck Society is gratefully acknowledged. In addition, we gratefully acknowledge funding through the Deutsche Forschungsgemeinschaft (DFG, German Research Foundation) through TRR 288–422213477 (project A10) and the SFB 1143 (project-id 247310070; project C09). Research in Dresden benefits from the environment provided by the DFG Cluster of Excellence ct.qmat (EXC 2147, project ID 390858940). Work at the Ames National Laboratory was supported by the U.S. Department of Energy, Office of Science, Basic Energy Sciences, Materials Sciences and Engineering Division. The Ames National Laboratory is operated for the U.S. Department of Energy by Iowa State University under Contract No. DEAC02-07CH11358.

AUTHOR CONTRIBUTIONS

E.G. designed the research. E.G., B.S., S.L.B., A.P.M., and P.C.C. performed the research. E.G. and B.S. wrote the manuscript with input from all authors.

FUNDING

Open Access funding enabled and organized by Projekt DEAL.

COMPETING INTERESTS

The authors declare no competing interests.

ADDITIONAL INFORMATION

Supplementary information The online version contains supplementary material available at <https://doi.org/10.1038/s41535-023-00596-1>.

Correspondence and requests for materials should be addressed to Elena Gati.

Reprints and permission information is available at <http://www.nature.com/reprints>

Publisher’s note Springer Nature remains neutral with regard to jurisdictional claims in published maps and institutional affiliations.



Open Access This article is licensed under a Creative Commons Attribution 4.0 International License, which permits use, sharing, adaptation, distribution and reproduction in any medium or format, as long as you give appropriate credit to the original author(s) and the source, provide a link to the Creative Commons license, and indicate if changes were made. The images or other third party material in this article are included in the article’s Creative Commons license, unless indicated otherwise in a credit line to the material. If material is not included in the article’s Creative Commons license and your intended use is not permitted by statutory regulation or exceeds the permitted use, you will need to obtain permission directly from the copyright holder. To view a copy of this license, visit <http://creativecommons.org/licenses/by/4.0/>.

© The Author(s) 2023